Shape-Memory Polyurethane/Multiwalled Carbon Nanotube Fibers

Qinghao Meng, Jinlian Hu, Yong Zhu

Institute of Textiles and Clothing, Hong Kong Polytechnic University, Hung Hom, Hong Kong

Received 18 December 2006; accepted 16 March 2007
DOI 10.1002/app.26517
Published online 29 June 2007 in Wiley InterScience (www.interscience.wiley.com).

ABSTRACT: Shape-memory polyurethane/multiwalled carbon nanotube (SMP–MWNT) composites with various multiwalled carbon nanotube (MWNT) contents were synthesized, and the corresponding SMP–MWNT fibers were prepared by melt spinning. The influence of the MWNT content on the spinnability, fracture morphology, thermal and mechanical properties, and shape-memory behavior of the shape-memory polymer was studied. The spinning ability of SMP–MWNTs decreased significantly with increasing MWNT content. When the MWNT content reached 8.0 wt %, the fibers could not be produced because of the poor rheological properties of the composites. The melt-blending, extrusion, and melt-spinning processes for the shape-memory fiber (SMF), particularly at low MWNT contents, caused the nanotubes to distribute homogeneously and preferentially align along the drawing direction of the SMF. The crystallization in the SMF was promoted at low MWNT contents because it acted as a nucleation agent. At high MWNT contents, however, the crystallization was hindered because the movement of the polyurethane chains was restricted. The homogeneously distributed and aligned MWNTs preserved the SMF with high tenacity and initial modulus. The recovery ratio and recovery force were also improved because the MWNTs helped to store the internal elastic energy during stretching and fixing. © 2007 Wiley Periodicals, Inc. J Appl Polym Sci 106: 837–848, 2007

Key words: polyurethanes; stimuli-sensitive polymers; nanocomposites

INTRODUCTION

Shape-memory polymers (SMPs) have been widely researched and used in both academia and industry because of their low cost, good processability, high shape recoverability, and large range of shape-recovery temperatures and the easy control of the critical recovery temperature.[1–8] Shape-memory polyurethane exhibits a shape-memory effect resulting from the thermodynamic incompatibility between the hard segments (aromatic diisocyanates) and soft segments (aliphatic polyethers or polyesters). The hard-segment phase has a higher thermal transition temperature (T_{perm}), whereas the soft-segment phase has a transition temperature, the glass-transition temperature or melting temperature, that acts as a switching temperature (T_{trans}). When shape-memory polyurethane is deformed at a high temperature (T_{high}) between T_{trans} and T_{perm} (thermal draw) or at a temperature below T_{trans} (cool draw), the temporary deformation can be fixed once the shape-memory polyurethane is cooled to (or kept at) a low temperature (T_{low}) below T_{trans}. If it is heated to a temperature above T_{trans}, its original shape can be recovered under entropy elasticity.[3,4,6,9,10]

Shape-memory polyurethane fibers can be prepared by wet spinning, dry spinning, chemical spinning, and melt spinning. Shape-memory fibers (SMFs) have outstanding mechanical properties because of the molecular orientation. In addition, they may have many different special applications. The melt-spinning method requires no harmful dimethylformamide (DMF) or coagulation bath and is relatively economical with respect to the production cost. The SMPs used in melt spinning should have higher thermal stability, good rheological properties, and a relatively high molecular weight to achieve good-performance shape-memory polyurethane fibers. However, the prepared shape-memory polyurethane fibers usually are of much lower tenacity, and the measured shape-memory effect is practically not noticeable. Multiwalled carbon nanotubes (MWNTs) are excellent candidates for reinforcing SMFs and, accordingly, for improving shape-memory properties.[11–22] In this study, we incorporated MWNTs into a shape-memory polyurethane matrix by *in situ* polymerization. Through mechanical-stirring, ultrasonic-vibration, melt-blending, extrusion, and spinning processes, a relatively homogeneous distribution of MWNTs in shape-memory polyurethane was achieved. The spinnability, mechanical properties, shape-memory behavior, and thermal properties of the shape-

Correspondence to: J.-L. Hu (tchujl@inet.polyu.edu.hk).
Contract grant sponsor: Hong Kong Innovation Technology Funding (High Performance Advanced Materials for Textile and Apparel project); contract grant number: GHS-088.

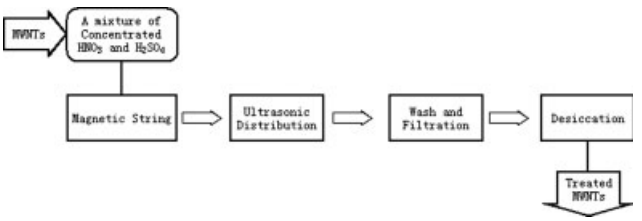

Figure 1 Schematic for preparing the MWNT used in the study.

memory polyurethane/multiwalled carbon nanotube (SMP–MWNT) fibers were then studied.

EXPERIMENTAL

Materials

MWNTs with an outer diameter of 10–20 nm, an inner diameter of 5–10 nm, and a length of $\sim$ 50 μm were supplied by Chengdu Organic Chemicals Co., Ltd. (Chinese Academy of Sciences, Chengdu, China). They were used after being treated by a mixed solvent of 70% nitric acid and 98% sulfuric acid (1.0 : 2.5 v/v) according to the literature[23] to improve the interfacial bonding with the polyurethane matrix. Figure 1 shows a schematic of the surface treatment of the MWNTs. The mixed solvent with MWNTs was heated to 140°C and kept there for 10 min (with mechanical stirring). Then, an ultrasonicator (Sonxi Co., Shanghai, China) with a power of 100 W and a nominal frequency of 50 kHz was used to distribute the MWNTs in the mixed solvent for 1 h. The treated MWNTs were collected by a glass filter (pore size = 500 nm) after being washed with sufficient distilled water repeatedly until the pH of the dispersion solution reached 7.0. The collected MWNTs were desiccated in a vacuum oven to remove the residual moisture. Then, they were stored in a desiccator containing phosphorous pentoxide before use.

The shape-memory polyurethanes were synthesized with polycaprolactone diol (PCL) as the soft segment, whereas diphenylmethane-4,4-diisocyanate (MDI) and the molecular extender 1,4-butanediol (BDO) were used as the hard segment. The polymer synthesis process and fiber preparation process are shown in Figure 2. All the glass vessels were cleaned and heated to remove any residual moisture. All the chemicals were demoisturized before use. MDI dimer or impurities that precipitated in the melt were removed before use. A calculated amount of modified MWNTs was predistributed in high-performance liquid chromatography-grade DMF. While the MDI melt was kept at 80°C, it was subjected to vigorous stirring for half an hour and ultrasonic vibration for 1 h. The shape-memory polyurethane was prepared by prepolymerization. BDO was added with vigorous stirring. The entire reaction was performed in a highly pure nitrogen environment. The reaction mixture was injected into a twin-screw extruder for further reaction, and the SMP–MWNT chips were then produced. The obtained polyurethane had a number-average molecular weight of 1.37×10^5, as measured by a high-performance liquid chromatograph (Waters Corp., MA) equipped with an Optilab rEX refractive index detector. SMP monofilaments of 40 denier were spun by a 20-mm single-screw extruder with highly pure nitrogen protection. The temperatures in the first zone, second zone, third zone, forth zone, extruder head, spinning pack, melt pipe, and pump were 180, 205, 208, 210, 212, 212, 212, and 212°C, respectively. The laminar air temperature was 22°C. The extruder head pressure was 5.00 MPa, and the spin pack pressure was 22.00 MPa. A spinneret with a single 0.4-mm hole was used. Then, the fiber passed two pairs of rollers at 80°C to release internal stress. The winding speed was 100 m/min.

Analysis and testing

Melt flow index

The melt flow index of our fibers was tested with a Davenport melt flow indexer MFI-10 (Fareham, UK). The samples were preheated in a barrel held at 210°C for 6 min. The amount of the polymer fed into the extruder was about 2.16 kg. The extruded polymer was cut every 60 s. The test was conducted five times and averaged for each polymer melt.

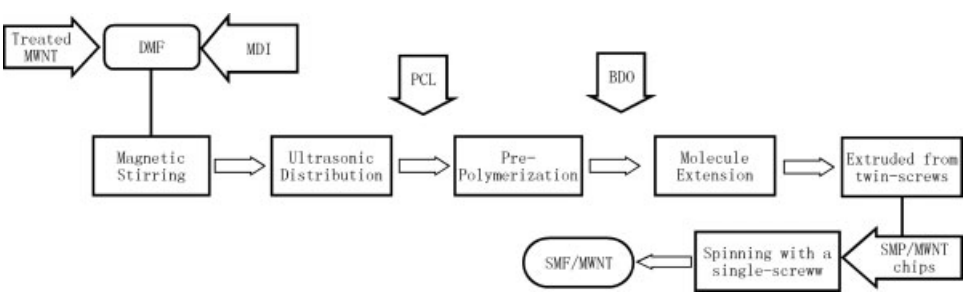

Figure 2 Schematic for preparing the SMP–MWNT fiber.

Scanning electron microscopy (SEM) and transmission electron microscopy (TEM) analysis

The monofilament surface images and fracture surface morphology of the prepared SMP–MWNT composites and SMP–MWNT fibers with different MWNT contents were taken with a Leica Stereoscan 440 scanning electron microscope (Cambridge, UK) operating at 20 kV. The fracture surface of the SMF composite was obtained as follows: a fiber was embedded in epoxy and then broken in liquid nitrogen. TEM images of the composite fibers were obtained with a Phillips CM 120 (Philips Ltd., Co., Eindhoven, The Netherlands). The SMP fiber was microtomed into two parts at 90° in the fiber axis direction with a diamond knife (Micro Star Co.) and a Reichert–Jung Ultracut microtome (at room temperature) (Heidelberg, Germany). The experiments were carried out at an accelerating voltage of 120 kV.

Differential scanning calorimetry (DSC) analyses

The thermal properties of the prepared fibers were investigated with a PerkinElmer Diamond differential scanning calorimeter with nitrogen as the purge gas. Indium and zinc were used for calibration. The samples were heated from −70 to 240°C at a rate of 10°C/min. They were then kept at 240°C for 1 min to remove the thermal history. Subsequently, they were cooled to −70°C at a cooling rate of 10°C/min. Finally, the fibers were reheated to 250°C to investigate the thermal properties.

X-ray diffraction (XRD) analyses

The XRD data were recorded with a Philips Xpert analytical XRD system at a voltage of 40 V, a current of 30 mA, and a radiation wavelength of 1.542 Å. Spectra were obtained in the Bragg angle (2θ) range of 10–40° with a scanning step size of 0.02° and a time per step of 1 s.

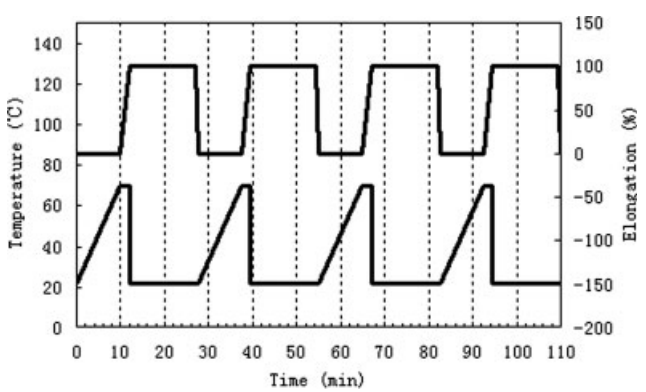

Figure 3 Programmed temperature–strain relations in the thermomechanical cyclic tensile test.

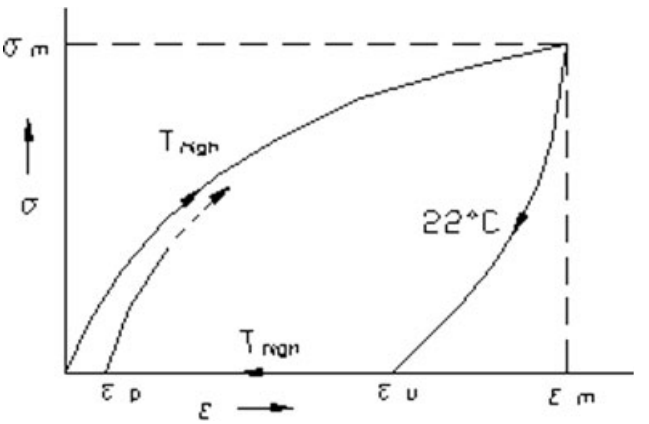

Figure 4 Schematic of a typical stress–strain curve of a thermomechanical cyclic tensile test.

Mechanical property testing

The mechanical properties of our SMF were measured with an Instron 4411 tensile tester according to ASTM Standard D 2256. The sample gauge length was 25 mm. The elongation speed was 300 mm/min. The measurements for each sample were conducted 10 times and averaged.

Thermomechanical cyclic tensile investigations

Thermomechanical cyclic tensile tests were carried out with an Instron 4466 tensile tester with a temperature-controlled chamber. In the measurements, the fiber had a gauge length of approximately 20 mm, T_{high} was set to 70°C, and the maximum elongation was 100%. The shape-memory test consisted of four procedures.

The programmed temperature–strain cycle is shown in Figure 3.[6] First, the fiber was heated to 70°C and was stretched to 100% strain at a speed of 10 mm/min at this temperature; second, the fiber was cooled to the ambient temperature (22°C), and the 100% strain was kept for 15 min; third, the clamp was unloaded, and the fiber was allowed to return to the original position at a speed of 40 mm/min; fourth, the fiber was heated to 70°C; and finally, the four procedures were repeated. This cycle was repeated four times for each fiber. The obtained stress–strain curves of the thermomechanical cyclic tensile tests are shown in Figure 4. ε_m is the maximum strain in the cyclic tensile tests, ε_u is the strain after unloading at T_{low}, and $\varepsilon_p(N)$ is the residual strain after recovery in the Nth cycle. The fixity ratio ($R_f(N)$) and recovery ratio ($R_r(N)$) at the Nth cycle and total recovery ratio after Nth cycle $R_{r\cdot tot}$ are calculated according to the following equations:[6]

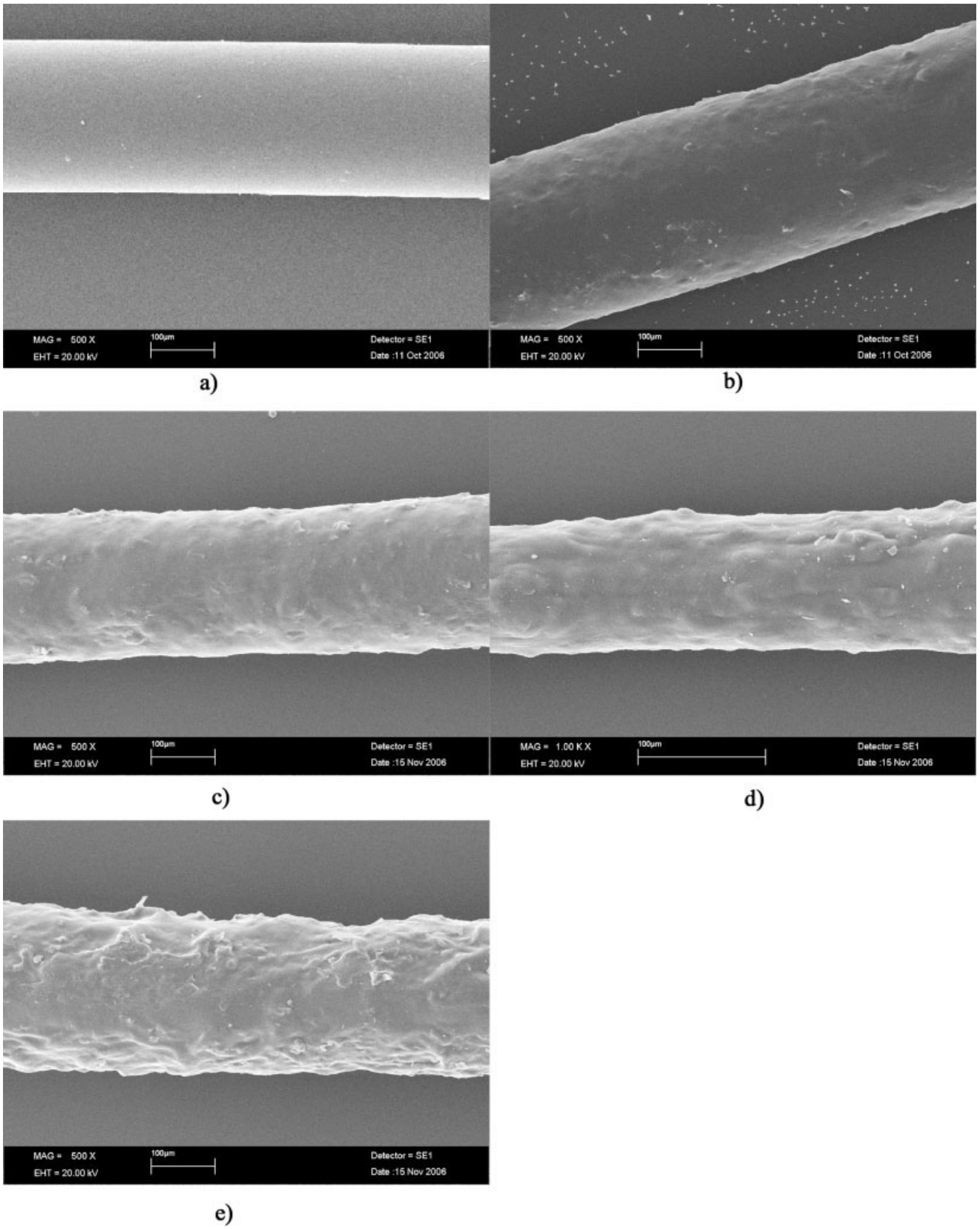

Figure 5 Influence of the MWNT concentration on the fiber surface quality: (a) 0, (b) 1.0, (c) 3.0, (d) 5.0, and (e) 7.0 wt %.

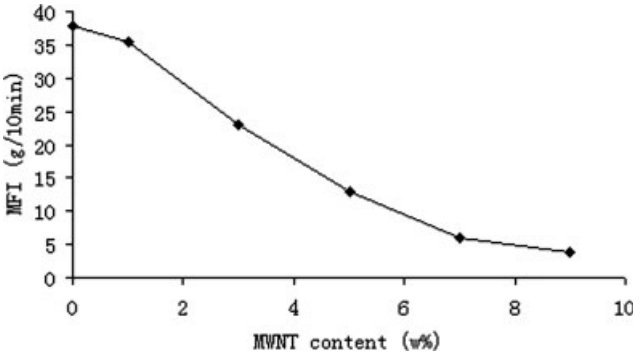

Figure 6 Relationship between the melt flow index (MFI) of SMP–MWNTs and the MWNT content.

$$R_f(N) = \varepsilon_u(N)$$

$$R_r(N) = [1 - \varepsilon_p(N)] - [1 - \varepsilon_p(N-1)] \times 100\%$$

$$R_{r,\text{tot}} = [1 - \varepsilon_p(N)] \times 100\%$$

RESULTS AND DISCUSSION

Spinnability

SEM images of fibers with different MWNT contents are shown in Figure 5. The surface of the SMP–MWNT fiber becomes rough and coarse with increasing MWNT content. When this content is increased from 3 to 5 wt %, the fiber surface becomes very coarse and has bad hand feeling. It is suggested that at an MWNT concentration of 5 wt %, some MWNTs aggregate and are exposed from the fiber surface.

The melt flow indices of the SMP–MWNT fibers with increasing MWNT contents are shown in Figure 6. The melt flow index of the composites decreases with increasing MWNT content. When the MWNT content is increased to 8 wt %, the rheological property of the composite deteriorates completely. Thus, the fibers cannot be spun. This can be ascribed to two factors: first, with increasing MWNT content, the continuity of the polymer matrix is destroyed, and second, the filter screens inside the spinneret are more readily blocked because of the high MWNT content. As a result, the spinnability of SMP–MWNTs having a high MWNT content is lowered.

Morphology study

Figure 7 presents an SEM image of the MWNTs used in the study. They were entangled together with long nanosize dimensions. The outer diameter was about 10–20 nm. Figure 8 presents SEM images of the SMP–MWNT fracture surface after *in situ* polymerization and the SMP–MWNT fiber fracture surfaces with an MWNT concentration of 1.0 or 5.0 wt %.

In SMP–MWNTs, many of the MWNTs are parallel to the sample fracture surface. However, in the SMP–MWNT fiber polyurethane matrix, most MWNTs are perpendicular to the fiber fracture surface, and this suggests that the MWNTs are preferentially aligned to the fiber axis. Besides, the MWNTs are distributed more homogeneously in the SMFs than those before the melt-blending process. To further prove the alignment distribution of MWNTs, a TEM investigation was conducted. Figure 9 presents TEM images of MWNTs in SMFs with concentrations of 1.0, 3.0, 5.0, and 7.0 wt %. The MWNTs are preferentially aligned in the fiber axis direction.

Figure 10 shows SEM images of SMP–MWNT fiber fracture surfaces with MWNT contents ranging from 0 to 7.0 wt %. At 1.0 wt %, the MWNTs can be distributed homogeneously in the shape-memory polyurethane matrix. When the MWNT content is 3.0 wt %, a little aggregation is observed. With an increase in the MWNT content, the MWNT distribution becomes inhomogeneous.

A model shown in Figure 11 is employed to explain the distribution and alignment effect of the shape-memory polyurethane induced by melt-extrusion and melt-spinning processes. In Figure 11, the soft segments of polyester are shown as being coiled or folded on themselves. The schematic section length of the zigzag line corresponds to one repeating unit within the polyol. The isocyanate is shown as a rigid circle. The hard segments are rigid and fixed, having a tendency to adhere to one another through strong hydrogen bonding. The MWNTs are entangled with polyurethane on a molecular level in the polymer matrix. In SMP–MWNTs, no significant polymer molecular orientation is observed. In SMP–MWNT fiber, on the other hand, the polymer molecules are oriented. During *in situ* polymerization, the treated MWNTs are predistributed in MDI by the ultrasonic process. The SMP molecular chains grow on the treated MWNT surface. As a result, the MWNTs better adhere to the shape-memory polyurethane matrix, especially to the hard segments (diisocyanates), by

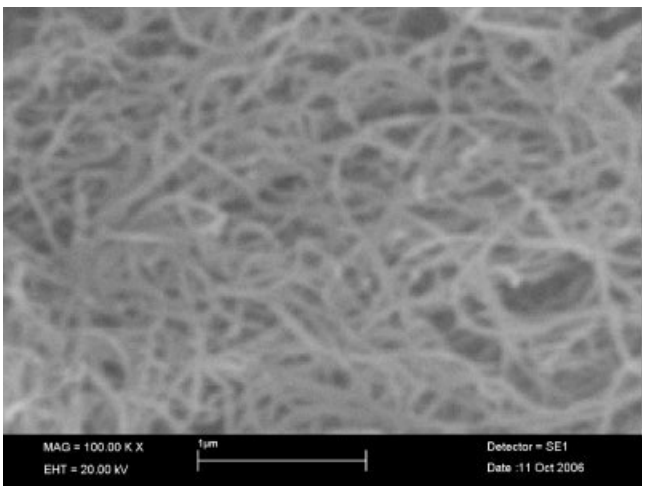

Figure 7 SEM image of MWNTs.

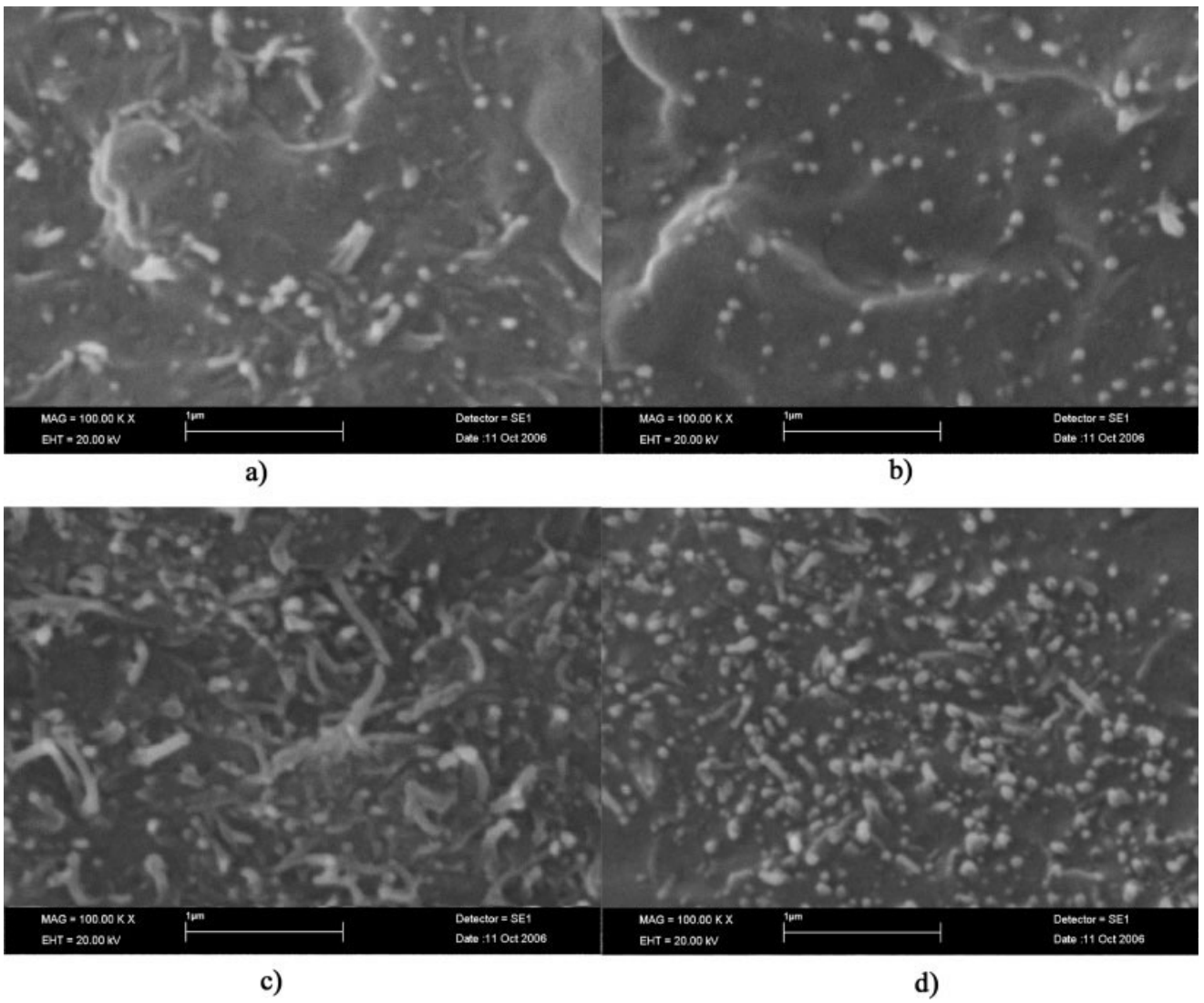

Figure 8 SEM images of the facture surfaces of the SMP–MWNTs and SMP–MWNT fibers after melt spinning: (a) SMP–MWNT with 1.0 wt % MWNT, (b) SMP–MWNT fiber with 1.0 wt % MWNT, (c) SMP–MWNT with 5.0 wt % MWNT, and (d) SMP–MWNT fiber with 5.0 wt % MWNT.

in situ polymerization in comparison with those obtained solely by melt blending. When SMP–MWNTs are heated above T_{trans}, the soft-segment phases are melted. If they are then stretched, the intact hard-segment phase has more interaction with the long nanosize MWNTs at this temperature. During melt blending, extrusion, and spinning, the higher shear force and drawing ratio contribute to the improved homogeneous distribution and axial alignment of the MWNTs. This alignment effect is more pronounced as the SMP is composed of soft and hard segments. The hard-segment phase is fixed by hydrogen bonds and stretches the curled MWNTs to align axially. As a result, the MWNTs adhere to the hard-segment domains effectively because they are nanosize in nature after being cooled to the ambient temperature.[24]

DSC and XRD results

Figure 12 presents the DSC curves of the fibers, and the data are summarized in Table I. All the samples show an endothermic peak at about 45°C, which can be attributed to the crystallization of the soft-segment phase.

The heat of fusion of the fiber having a low content of MWNTs (1.0 wt %) is slightly higher than that of the pure SMP fiber. The melting temperature of the 1.0 wt % MWNT fiber is also higher than that of the pure SMFs. It is suggested that a fiber having 1.0 wt % MWNT yields more oriented polymer chains and a more well-defined crystal structure. Thus, a small number of MWNTs act as nucleating agents that will enhance the crystallization process.[25] As can be seen

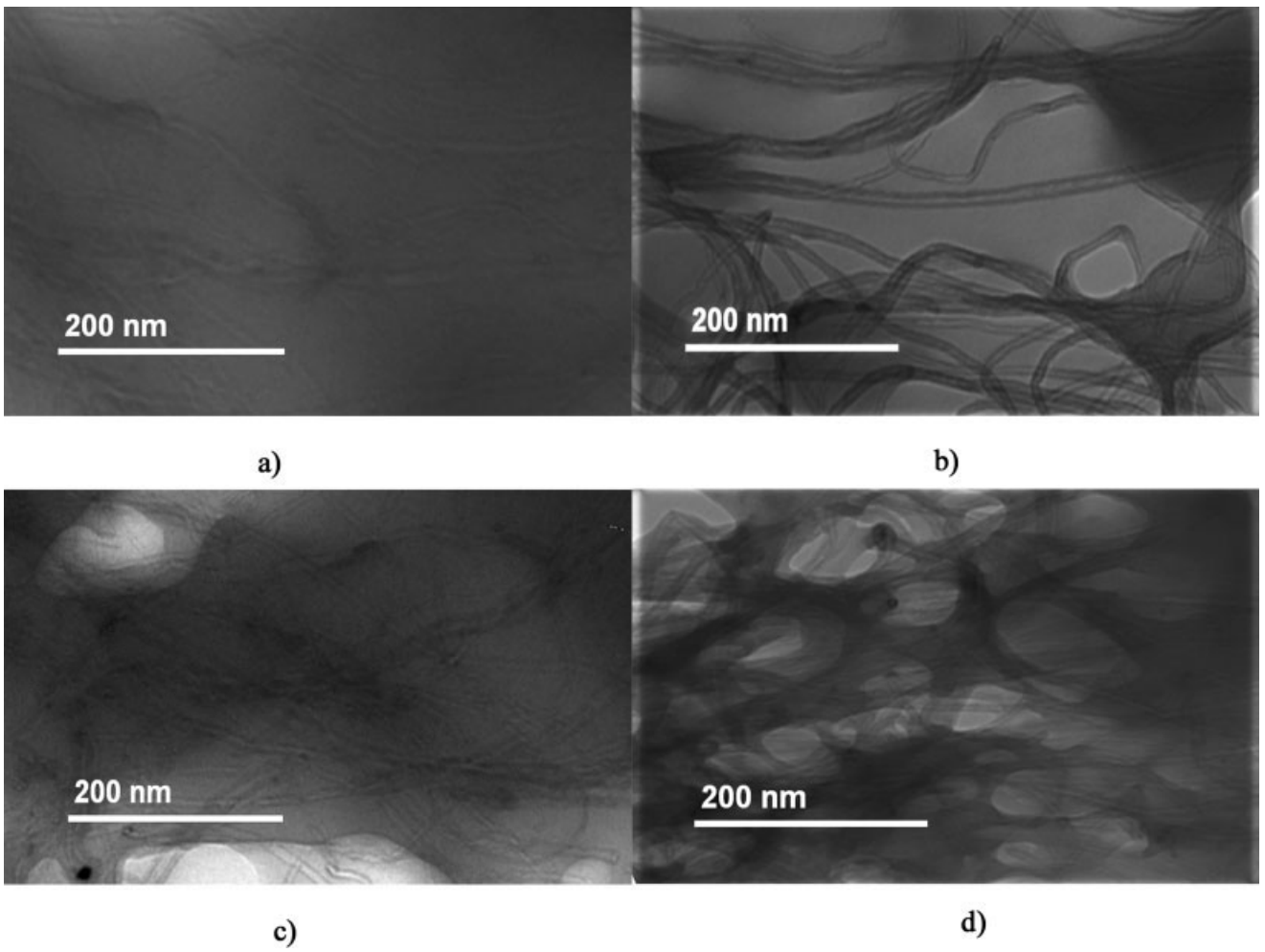

Figure 9 TEM images of the SMP–MWNT fibers with (a) 1.0, (b) 3.0, (c) 5.0, and (d) 7.0 wt % MWNT.

in Figure 12 and Table I, a further increase in the MWNT content decreases the fusion heat required by the fiber. This is because the increased MWNTs act as fillers, becoming a physical constraint on the SMP molecules, and thus lower the soft-segment mobility during crystallization. As a result, the degree of crystallinity and the melting temperature decrease.

To confirm the DSC results, XRD was also applied to measure the influence of MWNTs on the SMP–MWNT fiber crystallinity. The XRD patterns of PCL-4000, pure SMP fiber, and SMP–MWNT fibers with different MWNT contents are shown in Figure 13. In the wide-angle X-ray diffraction (WAXD) curve of PCL-4000, the diffraction peaks at 21.4, 22.1, 23.7, 36.1, and 38.5° are attributed to the PCL crystallization. However, in the XRD curves of SMP–MWNT fibers, the diffraction peaks at 22.1, 36.1, and 38.5° are not prominent. This suggests that in the SMF, the PCL crystallization is suppressed by the use of hard segments. From the XRD curves of the pure SMP fiber and SMP–MWNT fibers with different MWNT contents, it can be found that they all show diffraction peaks at 21.4 and 23.7°. The diffraction peak of SMP–MWNTs at a concentration of 1.0 wt % is a little higher than that of the pure SMP fiber. This suggests that the crystallinity of PCL in the SMP–MWNTs at a concentration of 1.0 wt % is higher than that in the pure SMP fiber. The PCL crystallinity decreases with continuously increasing MWNT contents. At 7.0 wt % MWNT, the diffraction at 21.4 and 23.7° broadens, and this proves that the crystals become very small.[26]

Mechanical properties

The stress, strain at break, and initial modulus of fibers with increasing MWNT contents are shown in Figures 14, 15, and 16, respectively. The tenacity of the fibers increases from 0.96 (pure SMP fiber) to 1.24 cN/dtex (fiber with 1.0 wt % MWNT). Continuously increasing the MWNT content may degrade the physical properties of the fiber. As can be observed in Figure 14, the tenacity of the fiber has a maximum value at about 1.0 wt % MWNT. Correspondingly, the elongation at break and initial modulus of the SMFs have decreasing and increasing trends, respectively, with increasing MWNT content.

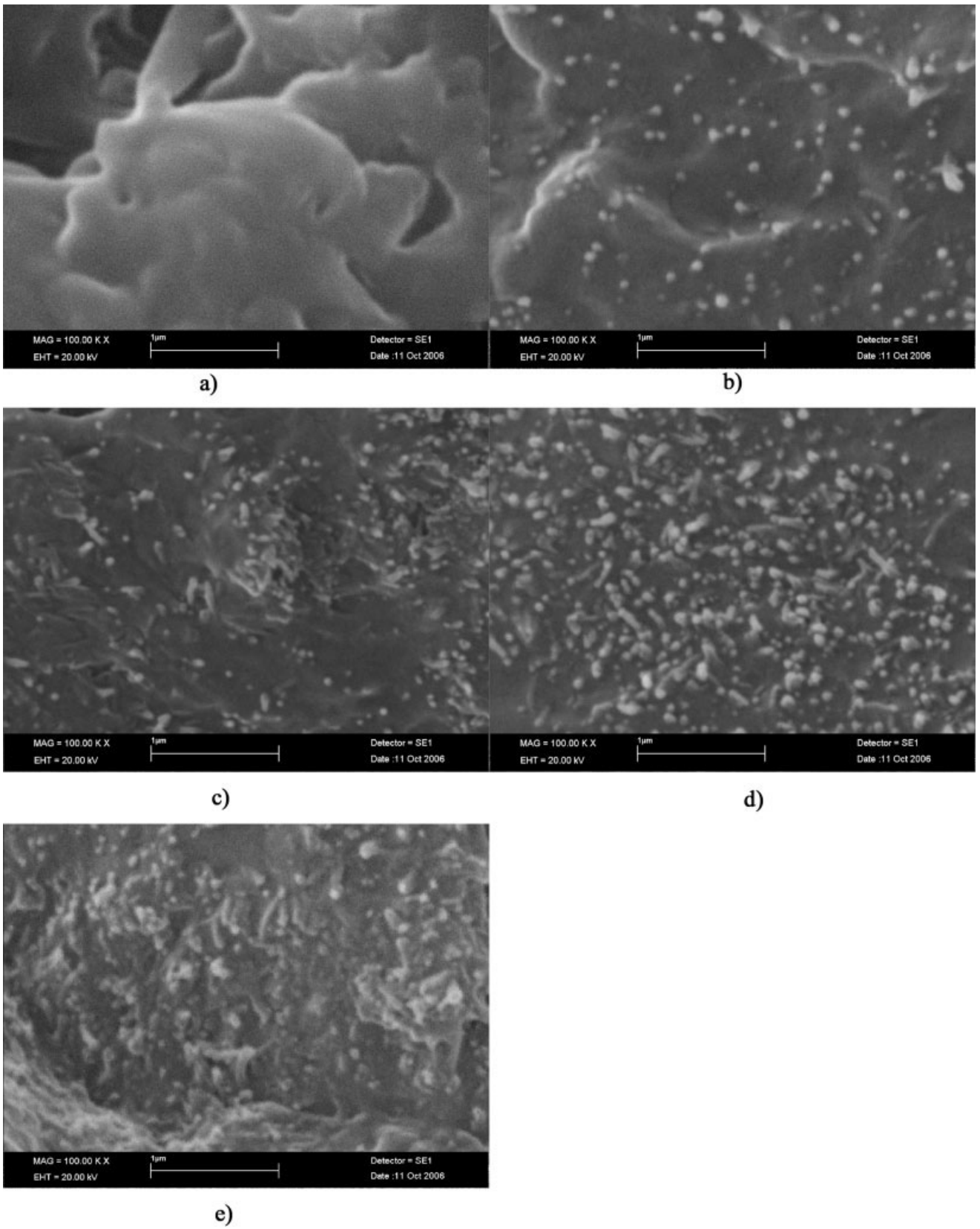

Figure 10 SEM images of the fracture surface of the fibers with (a) 0, (b) 1.0, (c) 3.0, (d) 5.0, and (e) 7.0 wt % MWNT.

During *in situ* polymerization, the treated MWNTs were distributed in the polyurethane matrix. The mixture was further blended by an extruder during the chip preparation and spinning process. Because the MWNTs were long and nanosized, they caused chain entanglement with the SMP molecules. During melt

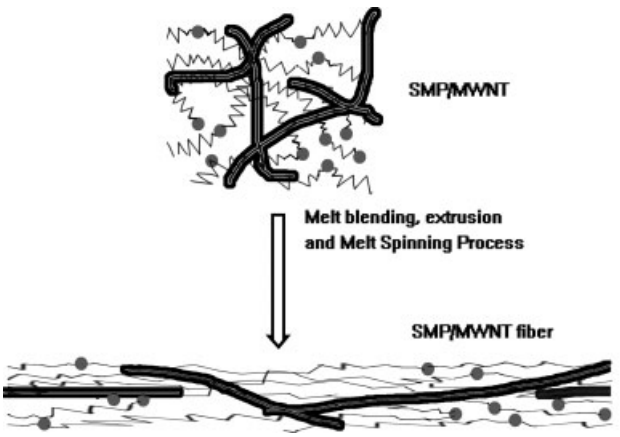

Figure 11 Schematic representation of the MWNT alignment in the SMP fibers after the melt-extrusion and spinning process.

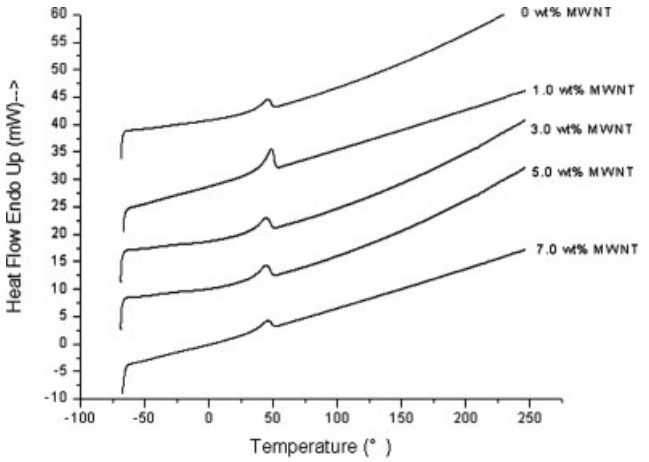

Figure 12 DSC thermographs of the SMP–MWNT fibers with different MWNT contents.

blending, extrusion, spinneret drawing, and post-drawing, the polyurethane molecules were oriented to some extent, and the MWNTs were also aligned preferentially along the axial direction of the fiber. At a temperature below the melting temperature of the hard segment but above the melting temperature of the soft segment, the hard segment had the effect of stretching the curled MWNTs. As a result, well distributed and axially aligned MWNTs were observed in the SMF matrix. The MWNTs treated by concentrated acid had high compatibility with the SMP matrix, particularly for the hard segments.[27] During the loading of the fiber, the stress was transferred to the high-modulus MWNT. As a result, the SMP–MWNT fibers with homogeneously axially aligned MWNTs had higher tenacity and initial modulus. Under these circumstances, the elastic deformation and molecular slippage were restricted. The elongation at break of the SMF decreased. With the increase in the MWNT content, the homogeneous distribution of MWNTs in the fiber was difficult to achieve. In addition, some of the MWNTs could not be covered by the polymer matrix. This degraded the mechanical properties of the SMP–MWNT fiber severely.

Shape-memory properties of the SMP–MWNT fibers

The thermomechanical cyclic tensile test was conducted to characterize the shape-memory effect of the SMP–MWNT fibers. The fixity ratio, recovery ratio, and maximum stress at 100% strain are shown in Figure 17, and the detailed shape-memory property results are tabulated in Table II. The fibers with different MWNT contents have fixity ratios of approximately the same shape. However, the influence of MWNTs on the fiber shape-recovery ratio is remarkable. The recovery ratio of the SMP–MWNT fiber is higher at 1.0 and 3.0 wt % MWNT than that of the pure SMP fiber. However, at 7.0 wt % MWNT, the shape-memory ratio is much lower than that of the pure SMF. The maximum stress at 100% strain increases monotonously.

For the SMP fibers, when the deformation is applied at a temperature higher than the melting temperature of the soft-segment phase, the SMP fibers are readily stretched. The recovery stress and recovery degree are mainly controlled by the hard-segment phase. For the SMP–MWNT system, the treated MWNTs, having better interaction with the hard-seg-

TABLE I
Results of the DSC Analysis of the SMP–MWNT Fibers

		SMP fiber			
	Pure SMP fiber	1.0 wt % MWNT	3.0 wt % MWNT	5.0 wt % MWNT	7.0 wt % MWNT
T_m (°C)	45.414	48.49	45.198	44.567	44.461
ΔH (J/g)	22.851	23.841	18.851	14.342	12.321
Crystallinity (%)	16.32	16.74	13.47	10.24	8.79

T_m is the crystal melting temperature, and ΔH is the heat of fusion. The soft-segment crystallinity was calculated from the enthalpy data of the crystallization with an enthalpy value of 142 J/g for the fusion of 100% crystalline PCL, as suggested by Crescenzi et al.[28,29]

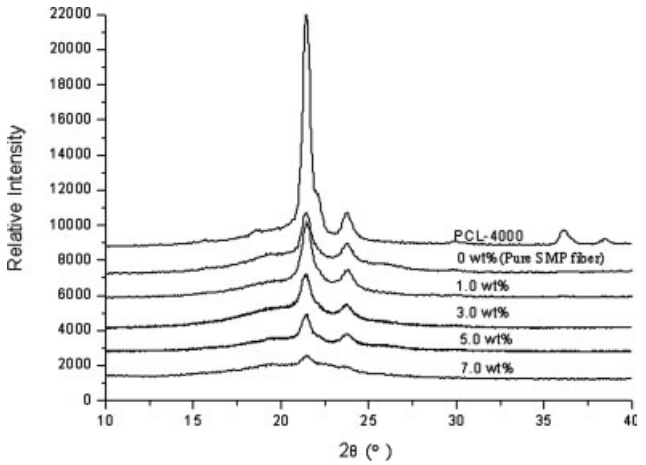

Figure 13 WAXD profiles of the PCL-4000, pure SMP fiber, and SMP–MWNT fibers with different MWNT contents.

ment phase, prevent the chain slippage of the polymer chains. Accordingly, the maximum stress at 100% deformation increases with increasing MWNT content. This indicates that the SMP–MWNT fiber is able to withstand higher stress at the same elongation, providing higher shape-recovery force to the fiber. On the other hand, the MWNTs, having better interactions with the shape-memory polyurethane molecules, particularly with the hard-segment regions, help to store the internal stress during stretching and shape fixing. As a result, the shape-recovery ratio increases. However, when the MWNT content is too high, the aggregated MWNTs degrade the fiber shape-recovery effect.

CONCLUSIONS

MWNTs were treated with a mixture of concentrated sulfuric acid and nitric acid to improve their compatibility with an SMP matrix before use. The MWNTs were predistributed in MDI via stirring and an ultrasonic process. The MWNTs were incorporated into the polyurethane by *in situ* polymerization. A further reaction was conducted in a double-screw extruder. SMP–MWNT fibers with different MWNT contents were prepared by a melt-spinning method. The influence of the MWNT content on the spinnability, fracture surface morphology, thermal properties, mechanical properties, and shape-memory properties was studied. The results suggested the following. First, the spinnability of the SMP–MWNT fiber decreased significantly with increasing MWNT content. When the MWNT content reached 7.0 wt %, the rheological property of the composite deteriorated, and the spinnability was lost. Second, the MWNTs were distributed homogeneously and aligned axially in the fibers, especially at MWNT fractions below 5.0 wt %, by the *in situ* polymerization, melt blending, extrusion, and melt spinning. Third, the MWNTs had an influence on the soft-segment crystallization process. When the content was low, they could act as nucleation agents for promoting crystallization. However, when the content was high, the crystallization was hindered. Fourth, the homogeneously distributed and axially aligned MWNTs endowed the fibers with high tenacity and initial modulus at low MWNT contents. The fiber tenacity increased from 0.96 (pure SMFs) to 1.25 cN/dtex (1.0 wt % MWNT). At high

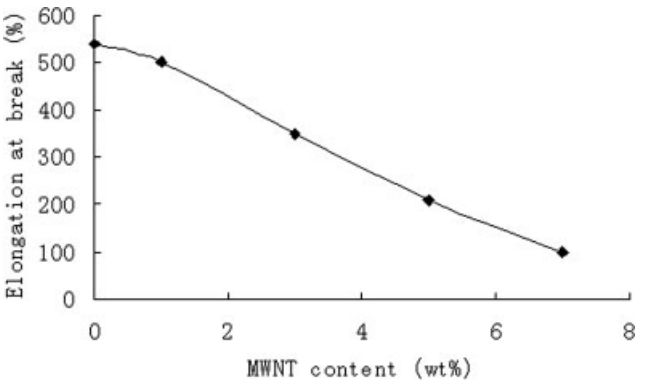

Figure 15 Relationship between the elongation at break of the SMP–MWNT fibers and the MWNT content.

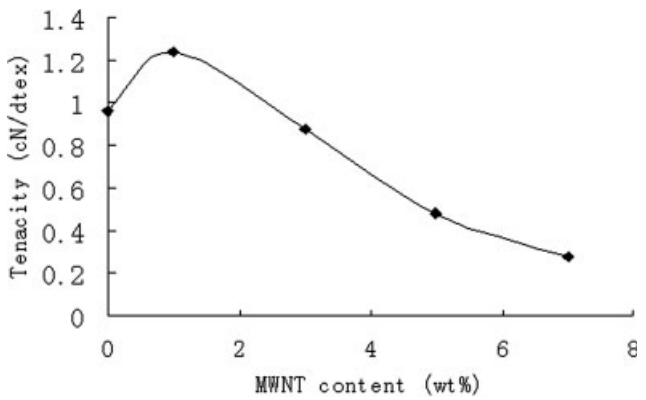

Figure 14 Relationship between the stress at break of the SMP–MWNT fibers and the MWNT content.

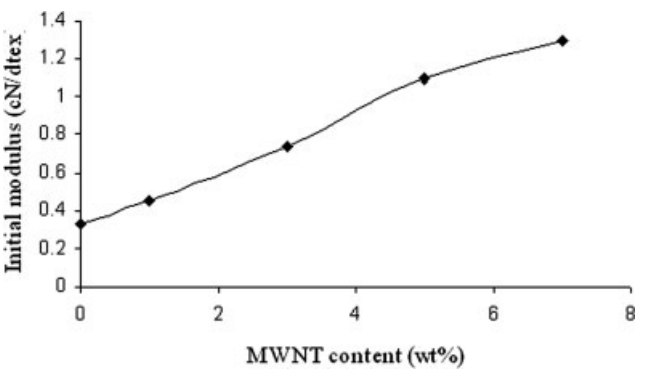

Figure 16 Relationship between the initial modulus of the SMP–MWNT fibers and the MWNT content.

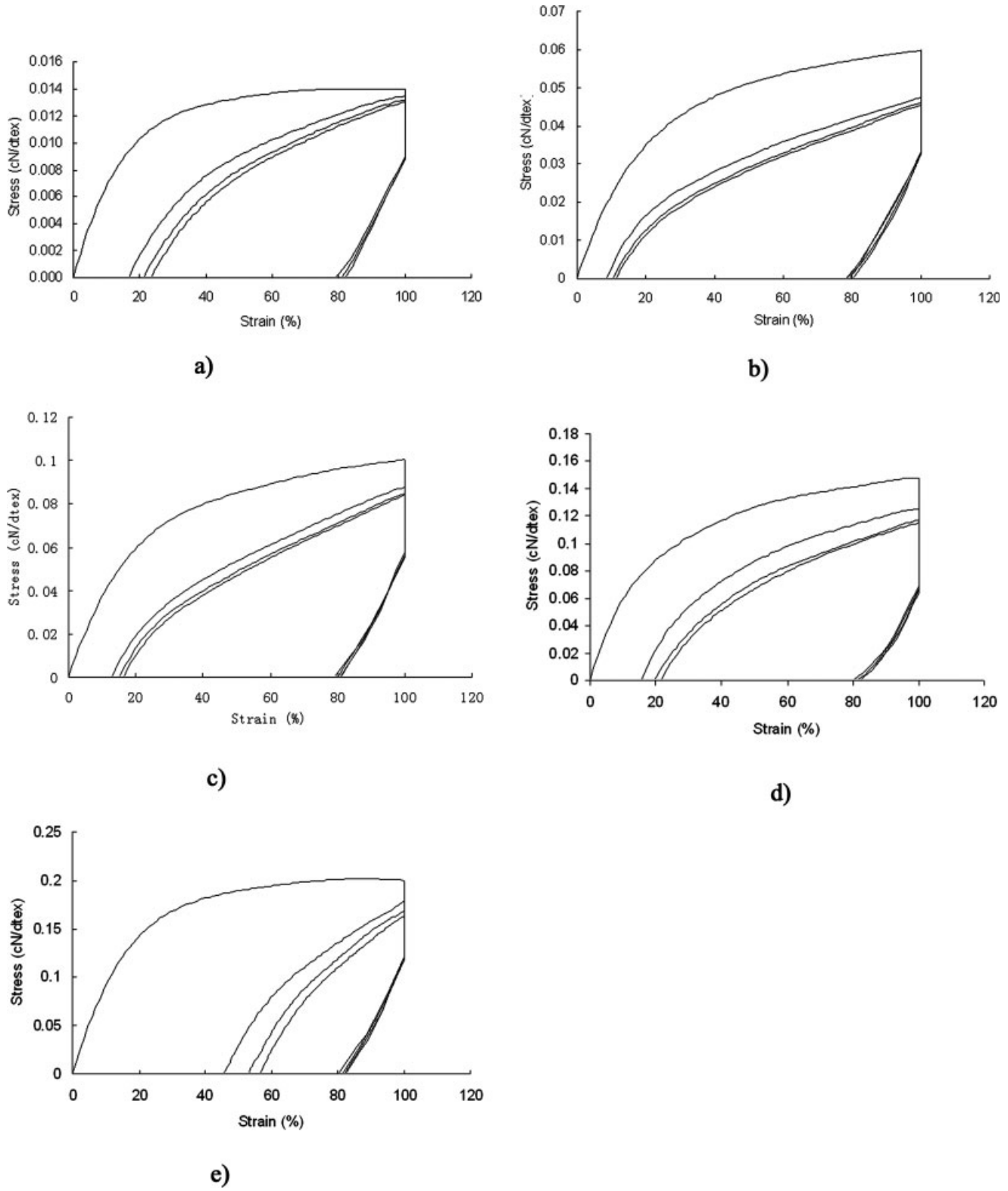

Figure 17 Thermomechanical cyclic tensile curves of (a) pure SMF and (b–e) SMP–MWNT fibers with 1.0, 3.0, 5.0, or 7.0 wt % MWNT, respectively.

MWNT contents, the aligned MWNTs aggregated and thus degraded the mechanical properties of the fiber. Fifth, the homogeneously distributed MWNTs helped to improve the shape-memory recovery ratio of the SMFs. The recovery ratio increased from 83 (pure SMP fiber) to 91% (fiber with 1.0 wt % MWNT). The shape-memory fixity ratio, on the other hand, was not changed significantly. The recovery force was

TABLE II
Thermomechanical Cyclic Tensile Results for the SMP–MWNT Fibers

	Circle	$\varepsilon_p(N)$ (%)	$\varepsilon_u(N)$ (%)	Stress at 100% strain (cN/dtex)	$R_{r,\mathrm{tot}}$ (N) (%)	R_r (N) (%)
0 wt % MWNT	1	0.0	79.2	0.0140	100.00	
	2	16.5	81.0	0.0134	83.50	83.5
	3	21.0	82.0	0.0132	79.00	94.6
	4	23.2	82.3	0.0130	76.80	97.2
1.0 wt % MWNT	1	0.0	78.0	0.0600	100.00	
	2	8.5	79.0	0.0475	91.50	91.5
	3	10.3	79.5	0.0462	89.70	98.0
	4	11.2	80.0	0.0460	88.80	99.0
3.0 wt % MWNT	1	0.0	79.0	0.1005	100.00	
	2	13.0	80.0	0.0880	87.00	87.0
	3	15.0	80.5	0.0850	85.00	97.7
	4	16.2	81.0	0.0840	83.80	98.6
5.0 wt % MWNT	1	0.0	80.0	0.0148	100.00	
	2	15.5	81.0	0.0126	84.50	84.5
	3	19.5	82.0	0.0117	80.50	95.3
	4	22.0	82.4	0.0115	78.00	96.9
7.0 wt % MWNT	1	0.0	80.5	0.2000	100.00	
	2	45.5	81.5	0.1800	54.50	54.5
	3	52.5	82.0	0.1680	47.50	87.2
	4	56.4	82.5	0.1620	43.60	91.8

also increased because of the interaction between the MWNTs and SMP, which helped to store the internal elastic energy during loading and shape fixing.

References

1. Hyashi, S. Int Prog Urethanes 1993, 6, 90.
2. Tobushi, H.; Hashimoto, T.; Ito, N.; Hayashi, S.; Yamada, E. J Intell Mater Syst Struct 1998, 9, 127.
3. Lin, J. R.; Chen, L. W. J Appl Polym Sci 1998, 69, 1563.
4. Lin, J. R.; Chen, L. W. J Appl Polym Sci 1998, 69, 1575.
5. Wei, Z. G.; Sandstrom, R.; Miyazaki, S. J Mater Sci 1998, 33, 3743.
6. Lendlein, A.; Kelch, S. Angew Chem Int Ed 2002, 41, 2034.
7. Yang, J. H.; Chun, B. C.; Chung, Y.-C.; Cho, J. H. Polymer 2003, 44, 3251.
8. Hu, J. L.; Ji, F. L.; Wong, Y. W. Polym Int 2005, 54, 600.
9. Kim, B. K.; Lee, S. Y. Polymer 1998, 39, 2803.
10. Liang, C.; Rogers, C. A. J Intell Mater Syst Struct 1997, 8, 285.
11. Biercuk, M. J.; Llaguno, M. C.; Radosavljevic, M.; Hyun, J. K.; Johnson, A. T.; Fischer, J. E. Appl Phys Lett 2002, 80, 2767.
12. Ounaies, Z.; Park, C.; Wise, K. E.; Siochi, E. J.; Harrison, J. S. Compos Sci Technol 2003, 63, 1637.
13. Jia, Z. J.; Wang, Z. Y.; Xu, C. L.; Liang, J.; Wei, B. Q.; Wu, D. H.; Zhu, S. 1999, 271, 395.
14. Cadek, M.; Coleman, J. N.; Ryan, K. P.; Nicolosi, V.; Bister, G.; Fonseca, A.; Nagy, J. B.; Szostak, K.; Beguin, F.; Blau, W. J. Nano Lett 2004, 4, 353.
15. Coopera, C. A. R. D.; Lipsb, D. A.; Mayerb, J.; Wagnera, H. D. Compos Sci Technol 2002, 62, 1105.
16. Lau Kin-Tak, H. D. Compos B 2002, 33, 263.
17. Lau Kin-Tak, H. D. Carbon 2002, 40, 1605.
18. Gong Xiaoyi, L. J.; Suresh, B.; Voise, R. D.; Young, J. S. Chem Mater 2000, 12, 1049.
19. Delmore, M. D.; Sholz, M. T.; Berman, M. A.; Bartical, D. C. U.S. Pat.6,077,240 (2000).
20. Lourie, O. W. H. Compos Sci Technol 1999, 59, 975.
21. Zhang Wei De, S. L.; Phang, I. Y.; Liu, T. Macromolecules 2004, 37, 256.
22. Sen Rahul, Z. B.; Perea, D.; Mikhail, I.; Hui, H.; Love, J. Nano Lett 2004, 4, 459.
23. Kwon, J.; Kim, H. J Polym Sci Part A: Polym Chem 2005, 43, 973.
24. McLean, R. S.; Sauer, B. B. Macromolecules 1997, 30, 8314.
25. Hu, S. M. J. L. J Elastomers Plast 2006, 38, 261.
26. Bittiger, H.; Marchessault, R. H. Acta Crystallogr B 1970, 26, 1923.
27. Jung, Y. C.; Sahoo, N. G.; Cho, J. W. Macromol Rapid Commun 2006, 27, 126.
28. Bogdanov, B.; Toncheva, V.; Schacht, E.; Finelli, L.; Sarti, B.; Scandol, M. Polymer 1999, 40, 3171.
29. Wunderlich, B. Macromolecular Physics: Crystal Melting; Academic: New York, 1980.